

Large-scale shoreline undulations and role of self-organization processes

Xiaojing Zhong^{1,†}, Ping Dong^{2,†} and Shenliang Chen^{3,*}

¹School of Engineering Technology, Jimei University, Xiamen 361021, China

²School of Engineering, University of Liverpool, Liverpool L69 3BX, United Kingdom

³State Key Laboratory of Estuarine and Coastal Research, East China Normal University, Shanghai 200062, China

This study investigates the large scale spatial variation behaviour of shoreline changes using the beach profile data along approximately 600 km shoreline around Hainan Island, China. It was found that there exists a power-law relationship between the mean shoreline change variance and the corresponding alongshore scale which holds up to 30 km for the annual shoreline change and reduces to 15 km for the seasonal shoreline change. The spatial and seasonal variations of shoreline azimuth, beach sediment size and wave conditions, and their connection with the shoreline change on different scales were studied. The results suggest that the internal feedback mechanisms between various processes with different spatial scales may be responsible for the observed shoreline change patterns, i.e. the annual shoreline behaviour on spatial scale 5–30 km is likely to be the result of self-organization, while the seasonal waves including tropical cyclones and storms exert dominant control of the morphological patterns at spatial scale of 10–25 km.

Keywords: Beach, forcing, power-law, seasonal, self-affinity.

COASTAL evolution involves complicated interactions and often exhibits self-similar (self-affine, fractal) patterns, which can be characterized by power-law scalings. The forms of these patterns are numerous (e.g. beach cusps¹, sand-bars^{2,3}, rip-channels⁴, and large scale shoreline patterns⁵) and vary in a wide range of spatio-temporal scale. Self-organized processes whose outcomes exhibit power-law scaling, are often observed and applied for modelling^{1,2,6} and can be easily explained if the spatial scales involved are relatively small. However, the power-law scaling that spans over a wide range of scales is much harder to interpret as self-organized patterns at different scales may be controlled by different physical processes. This means a unifying explanation for the relationship between variances of coastal morphological changes, such as horizontal movement of shoreline⁷ or change of shoreline curvature⁸ is presently not available. Therefore, to establish the scale relationships of morphological changes on coasts and underlying mechanisms for these

changes, investigations of coastal evolution in a wider range of scales is indispensable. In addition, a better understanding on the connection between power-law scaling and morphological self-organization on coast will be promoted accordingly.

While there exists a comparatively large number of studies on forced coastal forms, the self-organized behaviour of coastal morphology in a wide range of scales needs further exploration and research⁹. Based on the analysis of cross-shore profile changes in terms of their self-organizational properties, Southgate and Möller¹⁰ found that when wave conditions were weak or moderate, self-organizational (internal) processes determined the dynamics of the beach profile. The work of Tebbens *et al.*⁷ focused on shoreline change for tens of kilometers along of the northern North Carolina Outer Banks, United States. The log–log linear relationship between alongshore scale and the variance of horizontal shoreline position change in the cross-shore direction was found to hold for alongshore scales of approximately 100–1000 m. A follow-on study by Lazarus *et al.*⁸ extended the scale up to 8 km. These findings are important as it means that cumulative shoreline evolution process over a year or a few years may exhibit power-law scalings up to a length of 8 km although the underlying processes are unlikely to be scale free.

In this study, the power-law behaviour of shoreline changes at large spatial scales was investigated, and possible mechanisms to explain this behaviour were explored. The data of horizontal shoreline position change on beach profile used for this study were obtained from three beach profile surveys conducted in a 13-month period along the entire 600 km shoreline around Hainan Island, China. Wavelet analysis was applied to identify the power-law behaviour of horizontal shoreline position change and distinguish the shoreline change characteristics at different spatial scales. The standard empirical orthogonal function (EOF) analysis was applied on the elevation data of beach profile to study the variation characteristics of beach morphology in cross-shore direction at various coastal sections. The analysis results are discussed along with a set of hydrodynamic and geologic conditions in order to shed further light on the underlying mechanisms for the observed shoreline change patterns.

*For correspondence. (e-mail: slchen@sklec.ecnu.edu.cn)

†Equally contributed.

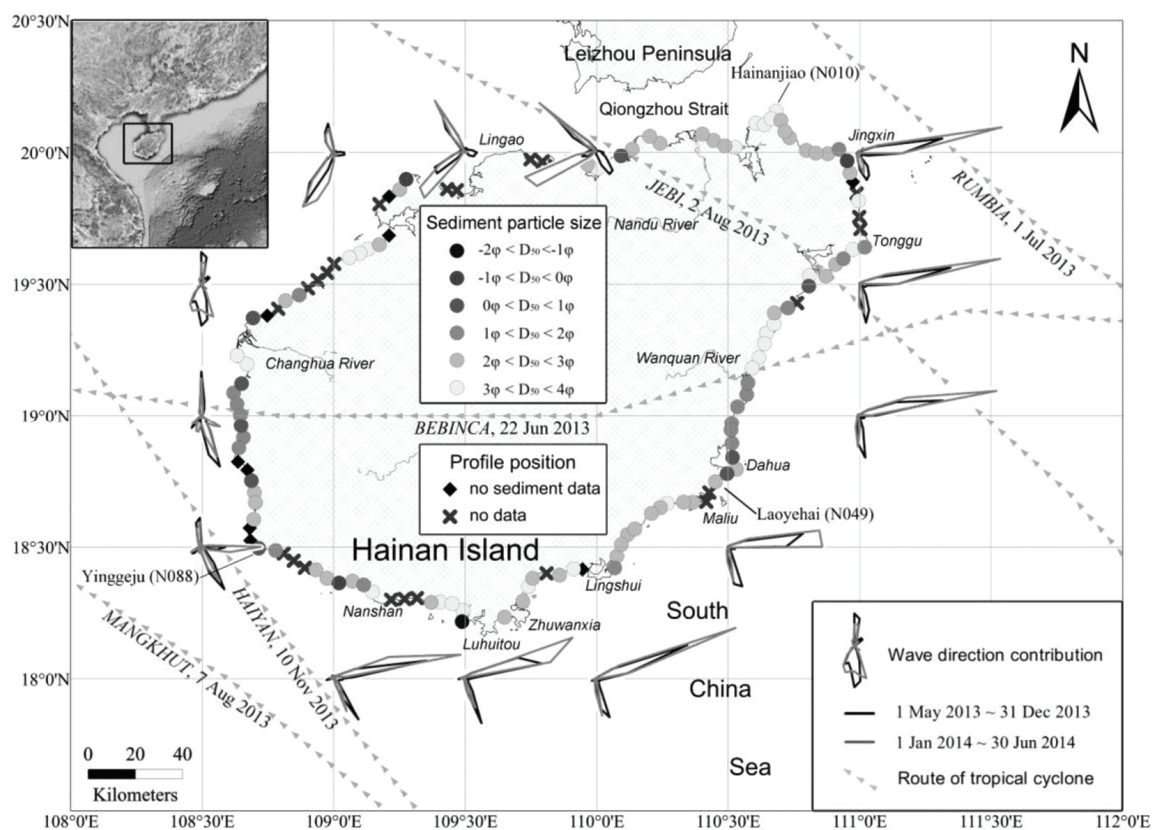


Figure 1. Location map of Hainan Island, wave direction contribution around Hainan and routes of tropical cyclones during the investigated period, particle size (D_{50}) of intertidal sediment collected in May 2013 and profile positions. Profiles are numbered N001 to N132 clockwise along the coastline.

Study area

Hainan Island is located in the South China Sea, separated from Leizhou Peninsula in the north by Qiongzhou Strait (Figure 1). Due to engineering works and urban development at Hainan Island, water and sediment fluxes of rivers on the island have decreased slowly over the past 50 years¹¹. At present, sediments involved in coastal evolution around Hainan Island mainly originate from the resuspension of deposited sediment and the erosion of backshore dunes¹². Sandy coasts are the main shoreline types, and they are separated by bedrock headlands and estuaries (Figure 1 and Table 1). From Hainanjiao to Laoyehai is the east coast with shoreline facing east, and from Laoyehai down to Yinggeju is the south coast.

The climate of Hainan Island and South China Sea is dominated by the East Asian monsoon, with northwest winds during October–March (winter), and south and southeast winds during April–September (summer)^{12,13}. The direction and energy of surface waves around the island are also closely correlated with the seasonal wind direction and forcing strength¹². Prevailing waves are from northeast in winter and southeast and southwest in summer. During summer, the Hainan Island is frequently visited by tropical cyclones (about 3 times per year)¹⁴.

Methods

Field survey and data

One hundred and thirty two profiles perpendicular to the local shoreline around Hainan Island were surveyed, and the distance between every two adjacent profiles was approximately 5 km (Figure 1). Profile elevation was measured with Trimble RTK-GPS 3 times in May 2013 (from 30 April to 14 May 2013), December 2013 (from 6 December to 21 December 2013) and June 2014 (from 6 June to 20 June 2014). The measuring error was less than 6 cm, which was much smaller than the magnitude of shoreline position variations involved. The latitude and longitude of each profile were recorded in the first survey, and then precisely located in the subsequent surveys. Mean sea level (MSL, 0-m contour) was taken as the representative shoreline position which can be easily and accurately determined by beach survey data¹⁵. The difference between distances from the fixed measuring points at the backshore of the profiles to MSL of the two surveys was then taken as the shoreline change. Among the three sets of data for comparison, May 2013–June 2014 (difference of shoreline position between June 2014 and May 2013) represents the annual variation of

Table 1. Major capes, rivers along coast of Hainan Island¹¹

Type	Water discharge*	Sediment discharge*	Name	Flank profiles
River	$5.673 \times 10^9 \text{ m}^3/\text{y}$	$3.877 \times 10^5 \text{ t/y}$	Nandu	N002, N003
Cape			Hainanjiao	N010, N011
Cape			Jingxin (Baohu)	N017, N018
Cape	$4.780 \times 10^9 \text{ m}^3/\text{y}$	$4.533 \times 10^5 \text{ t/y}$	Tonggu	N024, N025
River			Wanquan	N039, N040
Cape			Dahua	N047, N048
Cape			Maliu (Niumiao)	N051, N052
Cape			Lingshui	N061, N062
Cape			Zhuwanxia	N068, N069
Cape			Luhuitou	N069, N070
Cape			Nanshan	N077, N078
Cape			Yinggeju	N088, N089
River			$3.643 \times 10^9 \text{ m}^3/\text{y}$	$6.989 \times 10^5 \text{ t/y}$
Cape	Lingao	N125, N126		

shoreline while May 2013–December 2013 and December 2013–June 2014 are the seasonal changes of shoreline.

For each profile measured, five sediment samples were collected along the beach profile starting 2 cm from the top of the profile in the first survey. Sieve analysis was used to obtain particle size distributions of the samples, and Friedman series formulas¹⁶ were then employed to determine the median grain size (D_{50}) of each sediment sample. D_{50} values from the same profile were averaged to represent the sediment size for the profile.

Shoreline change analysis

The changes in MSL positions at 132 profiles constituted the shoreline change series around Hainan Island with missing data being filled by linear interpolation. The data was then reconstructed by wavelet transform, which provides information on both spatial and frequency dependence of a data series. The wavelet analyses were performed using the Wavelet Toolbox in Matlab R2010a. A filter (called Mexican hat wavelet) convolves with the shoreline change signal, and values for the scale parameter, a , are in the range 1–16. Since the profiles were distributed one after another around the Hainan Island, there was no beginning or ending of the shoreline change signal in the true sense. The profiles were named N001 to N132, and the terms N001 to N132 were then repeated three times in sequence to form the signal used for wavelet transform, that is: N001, N002...N132, N001, N002...N132, N001, N002...N132. Only the middle part of the coefficient series obtained was used, so that the results were not affected by the edge effect of wavelet transform. The power-spectral exponent, β , is the slope of the log–log plot of the variance of wavelet transform coefficients, V , and the wavelet scale, a .

Beach profiles analysis

The EOF analysis was applied to investigate beach profile features of different coastal sections at different

times. Each profile was transformed into a set of elevation data with a spatial interval of 1.5 m, starting from MSL. For unifying the length of different profiles, the landward blank elevation data were filled with the elevation of the farthest point measured, which usually is the highest point for shorter profiles. Hence there are 100 elevation variables on each profile while the unified profile length is 150 m. The 132 profiles, each with 100 elevation variables, constitute a multivariate matrix fed to the EOF analysis. For unified profile elevation data from the same survey, four beach topography data matrices used for the EOF analysis were obtained: one matrix contained all the profiles around Hainan Island (N001–N132), and three matrixes for east coast (N010–N049), south coast (N049–N087) and the north and west coast (N088–N009) separately. A total of 12 matrixes were generated for three surveys. The calculation procedures followed closely the work of Vincent *et al.*¹⁷.

Hydrodynamic and geological conditions

Routes of tropical cyclones were accessed from Best Track Data by RSMC Tokyo-Typhoon Center (www.jma.go.jp). Significant wave height and wave direction around Hainan during the investigated period were accessed from hourly forecast data of WaveWatch III (WW3) Global Wave Model (oos.soest.hawaii.edu/erddap), which considered the weather conditions including tropical cyclones. While the resolution of WW3 Global wave model was 0.5° of long./lat., the modelling points of wave conditions were mostly located in deep water or far away from the shoreline. Therefore, in analysing the wave effects on shoreline change patterns, the seasonal significant wave heights along coast of Hainan predicted by Zhou *et al.*¹⁸ were also used.

Since the surveyed beach profiles were perpendicular to local shoreline, the azimuths of these investigated profiles represent the orientation of the local shoreline around Hainan Island. Azimuths of studied profiles

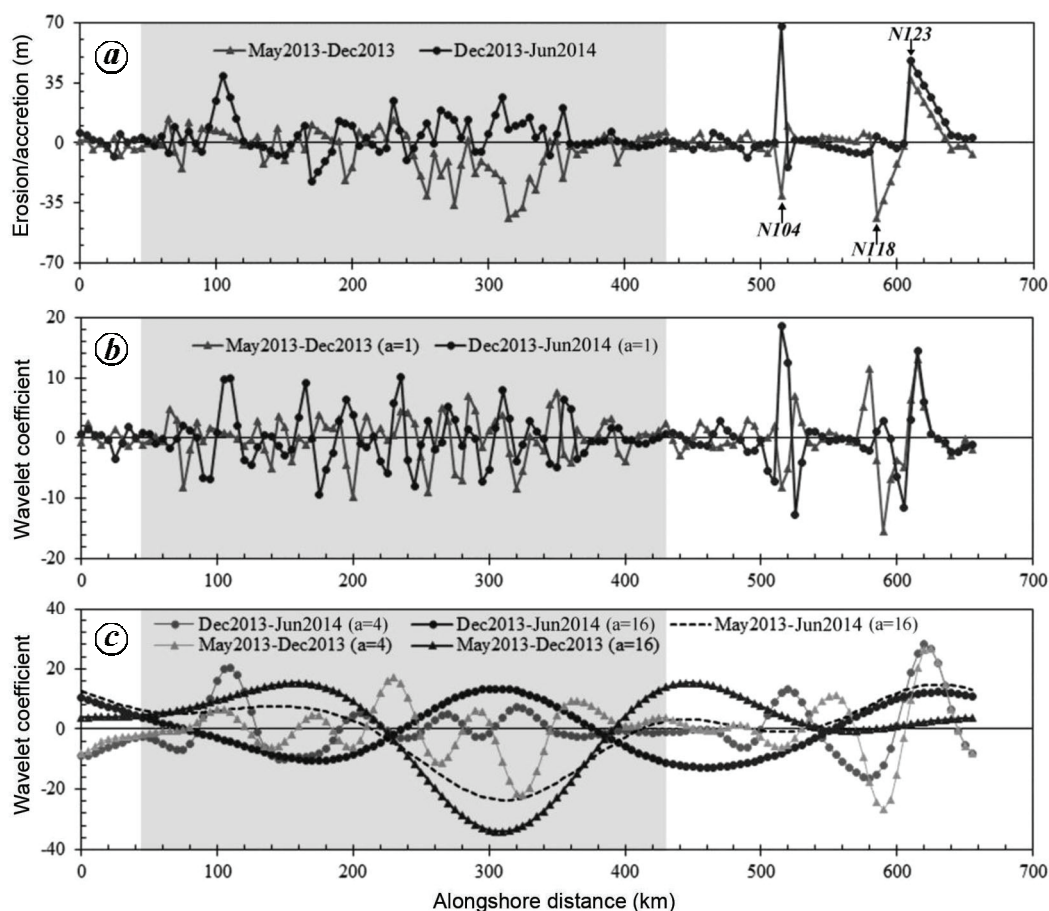


Figure 2. Shoreline change around Hainan Island and the results of wavelet analysis. *a*, Seasonal shoreline change of May–December 2013 and December 2013–June 2014. The ordinate axis indicates shoreline change (negative values – erosion). *b*, Wavelet transform results of seasonal shoreline change data with scale parameter $a = 1$. *c*, Wavelet transform results of seasonal and annual shoreline change data with scale parameters $a = 4$ and 16. The shaded parts are profiles from N010 to N087 (east and south coasts).

were calculated from GPS data. To examine the spatial scale of shoreline orientation variation along the coast, wavelet transform were used to analyse the azimuth data series.

Results

Rhythmic shoreline changes at different scales

Shoreline change signals exhibit a rhythmic pattern of alternating seaward and shoreward movements along-shore (Figure 2 *a*). At most survey positions, the shoreline moved in opposite directions in the two seasons (May–December 2013 and December 2013–June 2014) considered. The contrast between the wavelet transformed results of two seasonal shoreline change signals is also clearly evident (Figure 2 *b* and *c*): the coast which moved shoreward from summer to winter (May–December 2013) usually changed to moving seaward from the winter to

the following summer (December 2013–June 2014), and vice versa. The spatial periodic variations in the shoreline change series are clearly strong on different spatial scales.

The variations of shoreline change signals at different sections around Hainan Island were quite different as shown in Figure 2. The shaded parts are the south and east coast, and the cyclic variation there was more pronounced than the rest. In other words, the shorelines at south and east coast were more unstable than north and west coast, except for the three abnormal profiles (Figure 2 *a*): N104, N118 and N123. Profiles N104 and N123 have underwater shoal and mangrove, which may cause large changes in the local shoreline position. Profile N118 was affected by an artificial island located besides it, which was newly built after the first survey. Other profiles at north and west coast did not change much in shoreline position. Subsequent discussion will place particular emphasis on the south and east coast (profiles N010–N087).

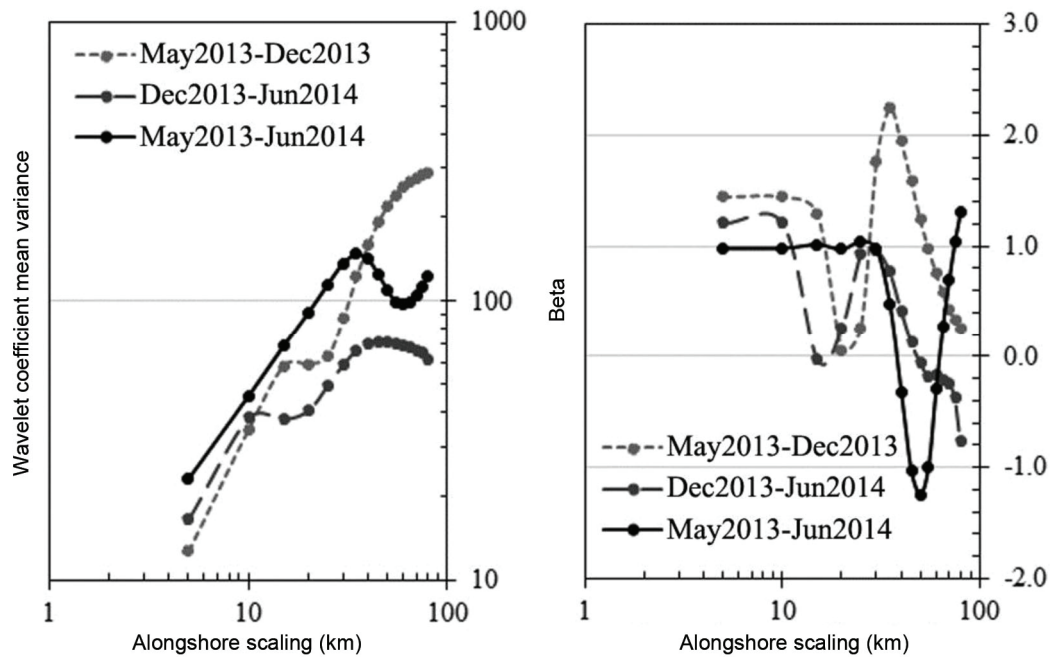


Figure 3. Log–log plots (left) and the corresponding power-spectral exponent β (right) relating wavelet coefficient mean variance of shoreline change to alongshore scale, for profiles N010 to N087. Wavelet width is multiplied by 5 km (distance between every two profiles) to get the alongshore scaling.

Relationships between wavelet coefficient variance and spatial scale of shoreline changes

The relationships between the wavelet transform coefficient variance and the spatial scale of shoreline change series at south and east coast are shown in Figure 3 by log–log plots. In the left graph, the wavelet coefficient variance of annual shoreline change, May 2013–June 2014, rises continually at alongshore scale from 5 km to 30 km, and increases again in the scale range of 60–80 km after dropping at 35–60 km. In contrast, the rising trends of seasonal change series, May 2013–December 2013 and December 2013–June 2014, break off in the scale range of 10–25 km, and then increase again up to a scale around 60 km. The power-spectral exponent β of annual shoreline change is steady over the scale range of 5–30 km. The power-law relationships of seasonal shoreline change are also strong with exponent β larger than 1 in the spatial scale up to 15 km.

Cross-shore profile change characteristics

The EOF analysis reveals that the first and second eigenvectors explain over 90% variation of profile elevation (Table 2). The first eigenvector shows the prevailing beach profile forms, and the second eigenvector reflects the subsequent beach elevation changes along the profiles. In Figure 4 *b* and *c*, it is clearly seen that the shapes of eigenvectors of winter profiles (December 2013) are

quite different from those of summer profiles (May 2013 and June 2014) for all profiles, which implies seasonal morphological changes on Hainan coasts.

The large variation of eigenvector weighting also indicates significant changes of beach profile, e.g. the second eigenvector weightings of profiles N40–N70 vary notably between surveys (Figure 4 *a*). On the other hand, profiles alongshore with close eigenvector weightings suggest that they have similar relationships with the eigenvector. Therefore subsections of the coast can be recognized by differences in the weightings on alongshore profiles, and the coastal sections divided on this basis correspond well with geological conditions (Table 1).

Hydrodynamic conditions

For the south and east coast of Hainan, the direction of incident wave in deep water was almost uniform alongshore with no discernable rhythmic patterns as seen in Figure 1. Furthermore, the annual significant wave height distribution in the coastal area considered was also rather similar, varying within the range of 0.6–1.2 m (Figure 5 *a*). As shown in Figure 1, along the east and south coast of Hainan, the prevailing wave direction was east-northeast in two seasons, while a proportion of waves coming from south in May–December 2013 changed to east in December 2013–June 2014.

During the survey period, there were five tropical cyclones that passed Hainan Island (Figure 1 and Table 3).

Table 2. Contributions of the first and second eigenvectors at different coast sections

	Profiles	May 2013	December 2013	June 2014
Contribution of first eigenvector (%)	N001–N132	87	88	89
	N010–N049	82	82	86
	N049–N087	89	90	91
	N088–N009	86	89	85
Contribution of first and second eigenvectors (%)	N001–N132	95	96	96
	N010–N049	91	93	95
	N049–N087	96	98	97
	N088–N009	95	96	95

All these cyclones approached Hainan from the east and south coasts between surveys in May 2013 and December 2013. The last cyclone that passed east coast was 4 months before the survey in December 2013 while the last cyclone affected the south coast only 25 days before 6 December 2013. Among the five cyclones, HAIYAN was the strongest and largest one (Table 3), and all of them were strong enough to affect the hydrodynamic conditions of some parts of Hainan coast. The cyclones generated high waves over a wide area, which can be recognized from wave conditions on both southeast coast and west coast (Figure 5 *b* and *c*). Based on the modelling wave conditions in 18.5°N, 110.5°E (*P1*) and 19°N, 108.5°E (*P2*), it can be concluded that the survey in December 2013 was affected by waves with relatively higher significant wave height induced by a series of storms, while the surveys in May 2013 and June 2014 were taken after a prolonged period of low waves.

Geological conditions

As shown in Figure 1, most profiles in the survey were on sandy beaches; only a few of them were covered by very fine gravel. It was also found that the sediments from each single bay were nearly of the same size, but differed significantly from the adjacent bays. The bays with alongshore length around 30–40 km were separated by protruding shoreline. As seen in Figure 6, at the spatial scales under 20 km, the variation trends of shoreline change and the azimuths were different from one another (Figure 6 *a*), and the Pearson product-moment correlation coefficient between them was only 0.21, which means they were barely correlated. At a scale of 40 km alongshore, the correlation was more discernible but remained weak (Figure 6 *b*) while at scale of 80 km alongshore (Figure 6 *c*), the azimuth displayed similar trends with shoreline change signal.

Discussion

The phenomena that shoreline changes driven by seemingly different processes can exhibit a consistent trend

across a wider range of scales in a power spectrum is indeed both interesting and hard to explain. Compared to previous studies^{7,8,19}, the scale of the present study area is much larger. The power-law relationship for the annual data implies that the self-affine property of shoreline changes can exist over four orders of magnitude in along-shore scale, from 10 m to 3×10^4 m. As this wide range of scales covers most spatial scales pertaining to the short and medium term coastal evolution, the results suggest that shoreline movements within these scales could be strongly affected by nonlinear shoreline change dynamics including some forms of self-organization.

Since the concept of ‘self-organization’ was introduced by Werner and Fink¹ in their study of beach cusps, models involving self-organization have largely focused on the explanation for the formation of rhythmic features at specific spatial scales, from metres to over 100 km under a prescribed background hydrodynamic condition²⁰. It remains unclear how the self-organization or a combined forced and self-organization mechanism may be used to explain the dynamic changes of shorelines that exhibit power-law scaling²¹. The shoreline change patterns around Hainan Island revealed in this study may provide useful information about spatial and temporal boundaries between self-organization and forcing processes.

Self-organization behaviour of coastal morphology

For a complex system involving many processes with different scales which interact on the overlapping spatial scales, the peaks of the shoreline-change power spectra occurring at specific scales may indicate a possible transition of dominant processes. However, this does not preclude the possibility of a well-organized system with different processes across different scales. For temporal scale one year and spatial scale up to 30 km (May 2013–June 2014), the shoreline change seems to be a result of well-organized system with smooth growth of spectra power along with scales. The strong seasonal hydrodynamic conditions can cause this trend to break, with a temporal scale of half year and a spatial scale of 10–25 km. The evaluation of affecting factors/processes,

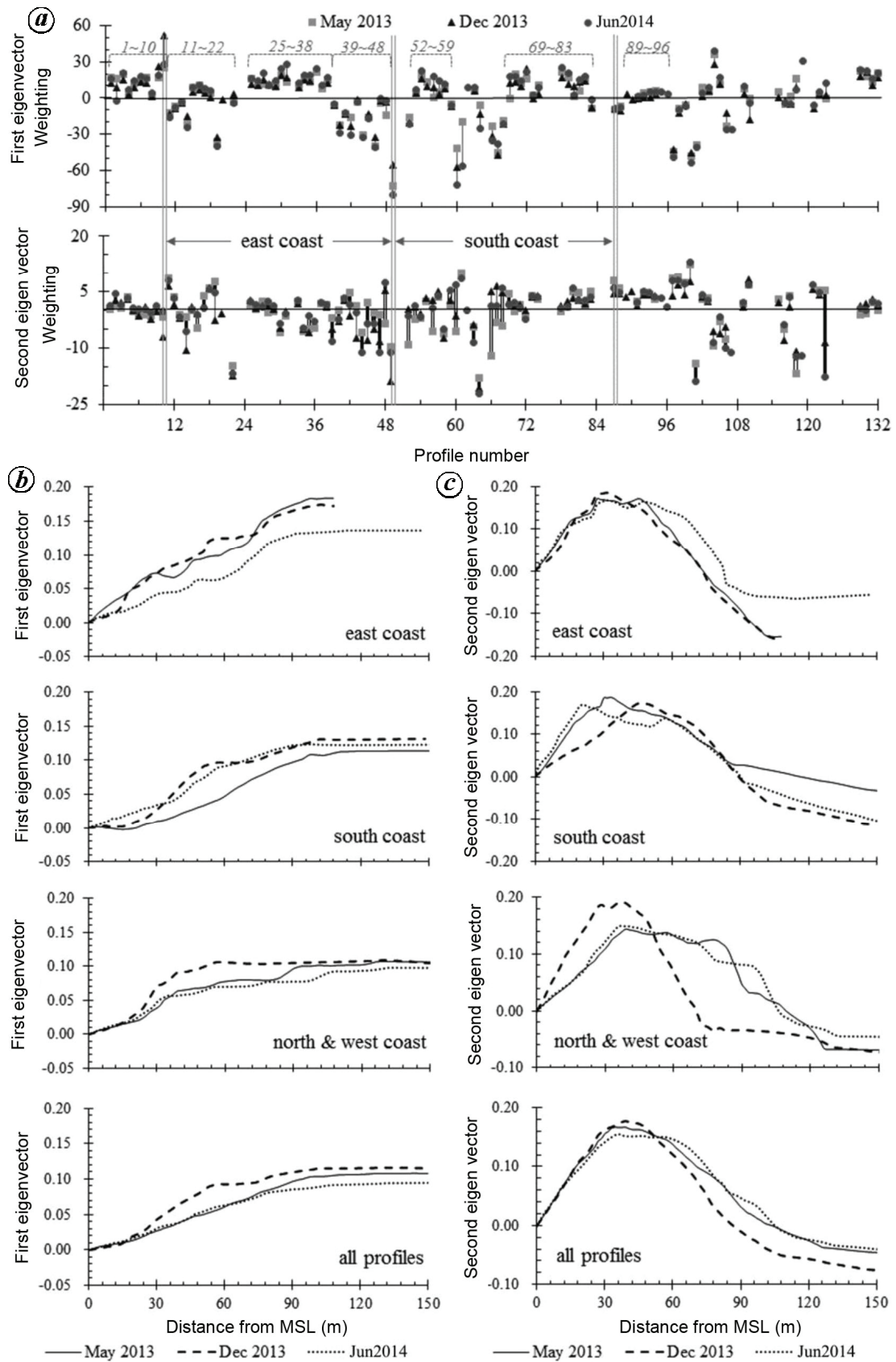


Figure 4. EOF analysis of beach profiles around Hainan Island. *a*, The weightings of the first and second eigenvectors on each profile in three surveys. *b*, First eigenvector of beach profiles. *c*, Second eigenvector of beach profiles.

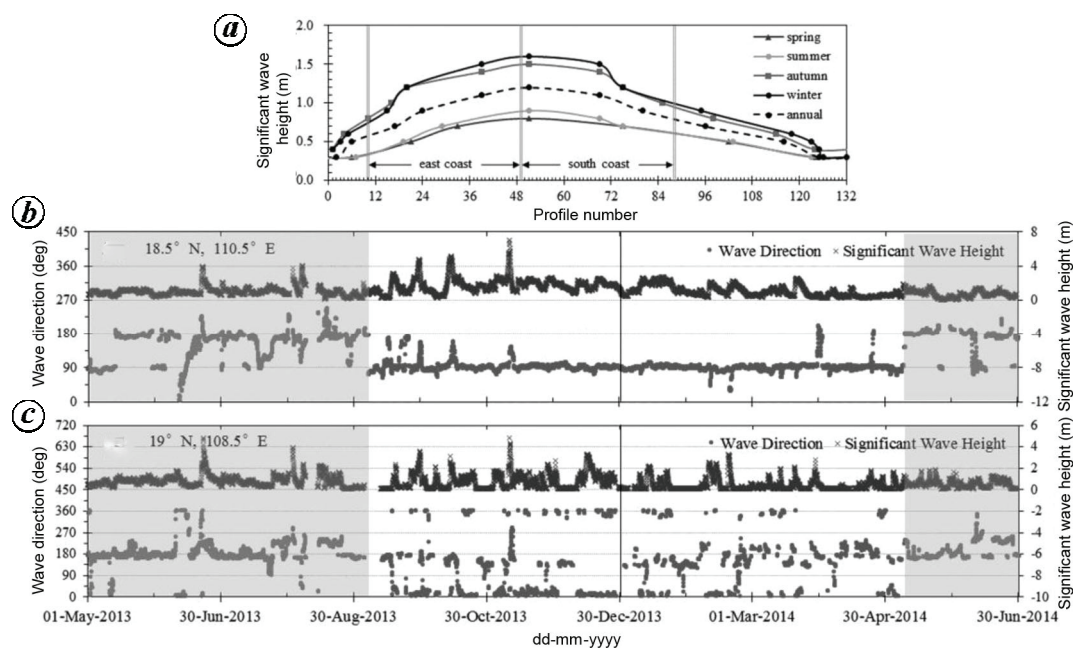


Figure 5. Model results of wave conditions around Hainan. *a*, Seasonal significant wave height distribution around Hainan Island, modelled by Zhou *et al.*¹⁸. *b* and *c*, Wave direction and significant wave height at 18.5°N, 110.5°E (south-east of Hainan) and at 19°N, 108.5°E (west of Hainan) during survey period, modelled by WaveWatch III (WW3) Global Wave Model.

Table 3. Parameters of tropical cyclones passed Hainan Island during study period (based on Best Track Data by RSMC Tokyo – Typhoon Center)

Tropical cyclone	Maximum sustained wind speed (knot)	Minimum central pressure (hPa)	Longest radius of 30 kt winds or greater (nautical mile)	Shortest radius of 30 kt winds or greater (nautical mile)
BEBINCA	40	990	150	120
RUMBIA	50	985	180	150
JEBI	50	985	250	150
MANGKHUT	40	992	120	120
HAIYAN	125	895	270	180

weak or strong, relies on the temporal and spatial scales considered.

Within alongshore scale 5–30 km, none of azimuth, sediment or deep water wave shows strong correlations with shoreline change (Figures 1 and 6, east and south coast). This indicates that there does not exist a dominant process that is due to any of these factors in the system. The system evolves mainly through internal feedback mechanisms between processes with different spatial scales, i.e. through self-organization. And the peaks of spectrum around scale 30 km and beyond are more likely to be due to other controlling factors of the system.

Controlling role of seasonal hydrodynamic conditions at the scale of 10–25 km

Based on the modelling wave data, tropical cyclones can generate high waves over a large sea surface area:

distance between *P1* and *P2* is more than 200 km but high waves driven by cyclones can be easily identified in both positions. The shoreline change in May–December 2013 showed little erosion on east coast and only a part of the south coast was seriously eroded. This may be due to the time intervals between the tropical cyclones and the survey, because the cyclones impacted east coast 4 months before the survey in December. Their effects have diminished as a result of beach recovery during this period, but the last storm passed south coast in November which was expected to leave a much greater impact on shoreline measured in December.

As expected, high waves induced by cyclones and winter storms can destroy shoreline patterns that had already formed through self-organization process prior to these events after which beach recovery and evolution would resume. This is especially the case for shoreline changes in May–December 2013 data. Through self-organization process spatial shoreline patterns tend to grow with time

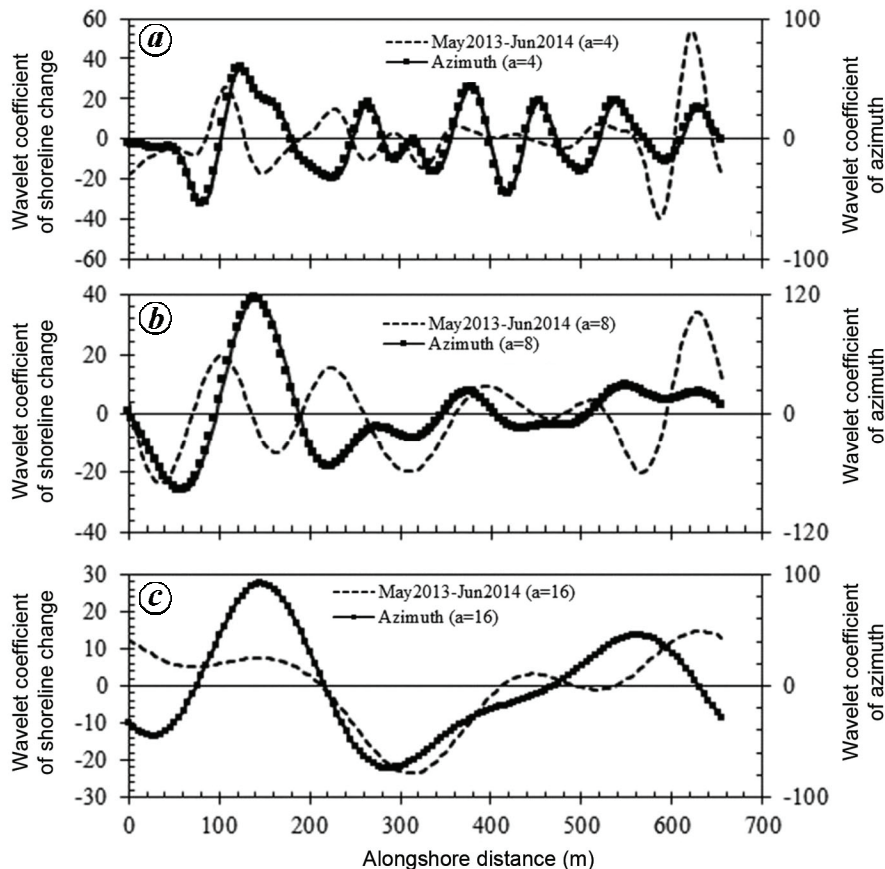


Figure 6. Wavelet analysis of annual shoreline change, azimuth and submerged slope of alongshore profiles. Wavelet coefficients of azimuth are divided by three for plotting in figures. Submerged slope is calculated between elevations 0 and -5 m at each profile.

and larger scale patterns require longer time to form than smaller ones²⁰. Although there were 1–4 months for shoreline to recover from impacts of tropical cyclones by December 2013, only smaller (less than 10 km) shoreline change patterns developed. Larger patterns beyond 10 km did not have sufficient time to form until June 2014.

Geological control at the scales over 30 km

Apart from self-organization and hydrodynamic forcing, the changes in background coastal settings can also affect the evolution of shoreline, an effect which is often referred to as geological control²². Although the correlation is weak between datasets of shoreline change and azimuth, the variation patterns do show similar trends on large scales. Beyond the alongshore scale of 30 km, the coastline variation resulted from the cumulative effects of interactions between hydrodynamic forcing and geological features. As seen, shoreline of Hainan Island is divided by various protruding headlands into beach sections of different orientations (Figure 1). While the incoming wave direction from South China Sea is fairly uniform in space, the intersection angle of the wave is related to the

orientation of the local shoreline. Consequently, the sections that have different orientations are affected differently by these hydrodynamic conditions. As a result, the coast sections in four different directions can be clearly identified from the wavelet transform results as shown in Figure 6 c.

Conclusions

Based on the shoreline change data collected at Hainan Island over a 13-month period, the analysis revealed that the power-law relationships between the mean variance and the length scale of the annual shoreline changes can hold up to an alongshore scale of 30 km which is several times greater than that found in the previous studies⁸. While there is no spatial pattern within the wave direction or significant wave height along the studied coast, the hydrodynamic conditions showed significant seasonal character. Five tropical cyclones showed strong impacts on east and south coasts of Hainan Island, and diminished the shoreline change patterns with alongshore scale of 10–25 km. Much of the effects on the shoreline evolution caused by the storm get averaged out over a time scale of

one year, as the long-term shoreline evolution is mostly a diffusive process with diminishing memory effects with time²³. In the time period of one year, the shoreline change patterns develop into larger spatial scale than seasonal shoreline change patterns, but it is confined by relatively closed bays at scale around 30 km. Furthermore, the coastal orientation changes are also found to be effective in alongshore scale from 40 km to 80 km, or even larger.

It should be pointed out that the shoreline change behaviour described has limits as it is based on a coarsely sampled shoreline data from only three surveys over a 13-month period. The results obtained may contain certain degree of uncertainty and are inevitably influenced by the particular morphological characteristics of Hainan Island. More sites with different coastal conditions and data resolutions (spatial and temporal) should be studied to further establish the scale relationships of shoreline changes on wave-dominated sandy coasts and underlying mechanisms for these changes.

1. Werner, B. T. and Fink, T. M., Beach cusps as self-organized patterns. *Science*, 1993, **260**, 968–971.
2. Garnier, R., Dodd, N., Falqués, A. and Calvete, D., Mechanisms controlling crescentic bar amplitude. *J. Geophys. Res.*, 2010, **115**, F02007.
3. Tiessen, M. C. H., Dodd, N. and Garnier, R., Development of crescentic bars for a periodically perturbed initial bathymetry. *J. Geophys. Res.*, 2011, **116**, F04016.
4. Dong, P., Chen, Y. Q. and Chen, S. L., Sediment size effects on rip channel dynamics. *Coast. Eng.*, 2015, 124–135.
5. Ashton, A. D. and Murray, A. B., High-angle wave instability and emergent shoreline shapes: 1. Modeling of sand waves, flying spits, and capes. *J. Geophys. Res.*, 2006, **111**, F04011.
6. Lazarus, E. D. and Armstrong, S., Self-organized pattern formation in coastal barrier washover deposits. *Geology*, 2015, **43**, 363–366.
7. Tebbens, S. F., Burroughs, S. M. and Nelson, E. E., Wavelet analysis of shoreline change on the Outer Banks of North Carolina: an example of complexity in the marine sciences. *Proc. Natl. Acad. Sci. USA*, 2002, **99**(suppl 1), 2554–2560.
8. Lazarus, E., Ashton, A., Murray, A. B., Tebbens, S. and Burroughs, S., Cumulative versus transient shoreline change: dependencies on temporal and spatial scale. *J. Geophys. Res.*, 2011, **116**, F02014.
9. Baas, A. C., Chaos, fractals and self-organization in coastal geomorphology: simulating dune landscapes in vegetated environments. *Geomorphology*, 2002, **48**, 309–328.
10. Southgate, H. N. and Möller, I., Fractal properties of coastal profile evolution at Duck, North Carolina. *J. Geophys. Res.: Oceans*, 2000, **105**, 11489–11507.
11. Yang, Z. H., Jia, J. J., Wang, X. K. and Gao, J. H., Characteristics and variations of water and sediment fluxes into the sea of the top three rivers of Hainan in recent 50 years. *Bull. Mar. Sci. Bull.*, 2013, **32**, 92–99.
12. Wang, B., Chen, S., Gong, W., Lin, W. and Xu, Y., *Formation and Evolution of the Embayment Coasts Around Hainan Island*, Ocean Press, Beijing, 2006.
13. Tchernia, P., *Descriptive Regional Oceanography*, Pergamon Press: Oxford, New York, 1980.
14. Zhang, K., Song, C. and Chen, Y., Records and disaster evaluation of typhoons in east Hainan Island in recent 50 years. *Met. Environ. Res.*, 2010, **1**, 102–104, 108.
15. Boak, E. H. and Turner, I. L., Shoreline definition and detection: a review. *J. Coastal Res.*, 2005, **214**, 688–703.
16. Friedman, G. M., Dynamic processes and statistical parameters compared for size frequency distribution of beach and river sands. *J. Sediment. Res.*, 1967, **37**, 327–354.
17. Vincent, L., Dolan, R., Hayden, B. and Resio, D., Systematic variations in barrier-island topography. *J. Geol.*, 1976, **84**, 583–594.
18. Zhou, L. M., Li, Z. B., Lin, M. and Wang, A. F., Numerical simulation of wave field in the South China Sea using WAVEWATCH III. *Chin. J. Oceanol. Limnol.*, 2014, **32**, 656–664.
19. Del Río, L., Gracia, F. J. and Benavente, J., Shoreline change patterns in sandy coasts. A case study in SW Spain. *Geomorphology*, 2013, **196**, 252–266.
20. Coco, G. and Murray, A. B., Patterns in the sand: from forcing templates to self-organization. *Geomorphology*, 2007, **91**, 271–290.
21. Murray, A. B. *et al.*, Geomorphology, complexity, and the emerging science of the Earth's surface. *Geomorphology*, 2009, **103**, 496–505.
22. Jackson, D. W. T., Cooper, J. A. G. and Del Río, L., Geological control of beach morphodynamic state. *Mar. Geol.*, 2005, **216**, 297–314.
23. Dong, P. and Chen, H., Wave chronology effects on long-term shoreline erosion predictions. *J. Waterw., Port, C-ASCE*, 2001, **127**, 186–189.

ACKNOWLEDGEMENTS. This study was carried out as part of a larger project funded by the Public Science and Technology Research Funds Projects of Ocean, China (Grant no. 201405037). The datasets were provided by State Key Laboratory of Estuarine and Coastal Research, ECNU, and requests for materials should be addressed to Shenliang Chen (slchen@sklec.ecnu.edu.cn). Financial support through a joint PhD programme awarded to Xiaojing Zhong by the Chinese Scholarship Council and University of Dundee, UK is gratefully acknowledged. The authors thank Jin Hu, Weiheng Zheng, Qing Chen and Wufeng Cheng for their contributions in the field work.

Received 4 March 2017; revised accepted 3 May 2018

doi: 10.18520/cs/v115/i4/729-738